Chemical Engineering Journal 257 (2014) 20–27

Contents lists available at ScienceDirect

Chemical Engineering Journal

journal homepage: www.elsevier.com/locate/cej

# Nitrogen enriched biochar modified by high temperature $CO_2$–ammonia treatment: Characterization and adsorption of $CO_2$

Xiong Zhang, Shihong Zhang *, Haiping Yang, Ye Feng, Yingquan Chen, Xianhua Wang, Hanping Chen

*State Key Laboratory of Coal Combustion, Huazhong University of Science and Technology, Wuhan 430074, Hubei Province, China*

## HIGHLIGHTS

- Raw biochar is obtained from the by-product of biomass fast pyrolysis for bio-oil.
- $CO_2$–ammonia treatment combines the advantages of both $CO_2$ activation and ammonification.
- The presence of $CO_2$ in $CO_2$–ammonia treatment can promote ammonification.
- Chemical adsorption dominates the high temperature adsorption process.

## GRAPHICAL ABSTRACT

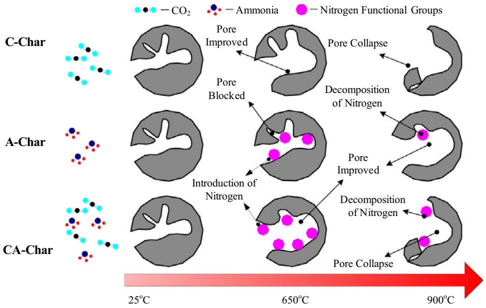

## ARTICLE INFO

*Article history:*
Received 10 June 2014
Received in revised form 4 July 2014
Accepted 7 July 2014
Available online 14 July 2014

*Keywords:*
Biochar
$CO_2$–ammonia modification
$CO_2$ adsorption
Deactivation model

## ABSTRACT

Adsorption is a promising method for $CO_2$ separation. The surface physical and chemical properties of adsorbent play a critical role during the adsorption process. Biochar, as the by-product from biomass fast pyrolysis for bio-oil, is renewable resources with good adsorption property. In this work, the adsorption behavior of biochar and its correlation with physical porosity and surface chemistry were investigated. A novel method for biochar modification by high temperature $CO_2$–ammonia mixture is proposed and compared with the conventional $CO_2$ activation and ammonia treatment. The results show that $CO_2$–ammonia modification combined the advantages of both $CO_2$ activation and ammonia treatment. The surface area of $CO_2$–ammonia modified chars is increased significantly up to about 627.15 $m^2/g$, and the ammonification (in the presence of ammonia) can introduce N-containing groups into the biochars (the N content up to 3.91 wt.% in $CO_2$–ammonia modified biochar). The breakthrough curve of $CO_2$ adsorption is fitted with deactivation model from the viewpoint of adsorption dynamics. The $CO_2$ adsorption capacity of biochar is proportional to the micropore volume at lower temperature (20 °C); however, it is dependent on the N content of biochar for $CO_2$ adsorption at higher temperature (120 °C).

## 1. Introduction

The increasing atmospheric $CO_2$ concentration is considered as a main contributor to global climate change in the past century [1]. $CO_2$ emissions are mainly caused by fossil fuel combustion, and coal accounts for roughly 25% of the world energy supply and 40% of the carbon emissions [2], so the $CO_2$ capture, usage, and storage (CCUS) from coal-fired power plant must be aggressively pursued [3]. While for secondary use or the geologic burial, $CO_2$ capture is a pivotal step. The current commercial technology for $CO_2$ capture is based on absorption using liquid amines, and the most commonly used amines are monoethanolamine and diethanolamine (MEA and DEA) [4,5]. However, the problems of high regeneration energy, large equipment size, solvent degradation,

---

* Corresponding author. Address: 1037 Luoyu Road, Wuhan 430074, Hubei, China. Tel.: +86 27 87542417; fax: +86 27 87545526.

*E-mail address:* shzhang@mail.hust.edu.cn (S. Zhang).

http://dx.doi.org/10.1016/j.cej.2014.07.024
1385-8947/© 2014 Elsevier B.V. All rights reserved.

and equipment corrosion make the process impractical for further applications [6]. In an effort to overcome the drawback of the liquid amine-based process, research has been focused on adsorption because of its low energy consumption and low equipment cost. Among all adsorbents, activated carbons are being proposed as suitable candidates for $CO_2$ capture since they are less sensitive to moisture, present a high $CO_2$ adsorption capacity at ambient pressure [7].

The adsorption properties of the activated carbon are not only determined by its micropore structure, but also surface chemistry [8]. Furthermore, the latter plays the most important role in the $CO_2$ adsorption performance at higher temperature [7,9]. The surface chemistry of activated carbon is governed by the presence of heteroatoms, such as oxygen and nitrogen. These heteroatoms exist in the form of acidic, basic or neutral functional groups [10]. Carbonaceous adsorbents can also benefit from delocalized $\pi$ electrons of aromatic rings and unsaturated valences [11]. A number of researches confirmed the enhancement in adsorption of acidic pollutants on modified activated carbon with increased basicity. In addition, alkaline activated carbon can also be used as catalyst in various chemical reactions [12]. Increment in alkalinity can be achieved through various techniques, such as impregnation [13–15], high temperature ammonification [16,17] and plasma treatment [18–20]. Among those, impregnation with proper chemicals is one of the most frequently used technologies. However, it is worth to note that the introduction of additives by impregnation might lead to some other negative effects. As reported, impregnated activated carbon with additives solution might block the pores in activated carbon; consequently, cause the decrement of the adsorption capacity [7,21,22]. Furthermore, the technique does not stabilize basic additives on the surface [23]. To overcome these disadvantages, heat treatment with the presence of ammonia gas was introduced to increase the basicity of activated carbon [16,24]. Mangun et al. [25] successfully prepared amine-rich activated carbon fiber (ACF) via high temperature ammonia treatment, and found that $C{=}N$ ($1600\ cm^{-1}$), $C{-}N$ ($1250\ cm^{-1}$), $C{\equiv}N$ ($2230\ cm^{-1}$) groups and cyclic amides ($1676\ cm^{-1}$) introduced onto the surface of ammonia-treated ACF. Przepiórski et al. [16] also found that N-containing groups were introduced into the carbon structure during ammonia treatment, but when the introduction of nitrogen content reached certain value, it can change the size of pores and close the micropore entries.

In order to maximize the introduction of nitrogen content and at the same time improve micropore structure, a novel method for increasing the $CO_2$ adsorption capacity of the adsorbent by combining high temperature ammonia treatment with $CO_2$ activation was proposed and testified in this work. Furthermore, considering cost and carbon–nitrogen cycle (a nitrogen-rich biochar that had adsorbed $CO_2$ could be used as the soil organic carbon, nitrogen fertilizer and nutrient for amending the soil quality) [26–29], raw biochar was derived from cotton stalk fast pyrolysis, and modified by three different approaches for developing efficient $CO_2$ adsorbents. Namely, conventional activation with $CO_2$, heat treatment with gaseous ammonia (referred to as ammonification) and the combination (referred to as activation and ammonification). The $CO_2$ adsorption process of biochar was discussed with deactivation model and the effect of the physico-chemical property on the $CO_2$ adsorption capacity of biochar was investigated.

## 2. Experimental

### 2.1. Sample

The biochar used in this work derived from cotton stalk fast pyrolysis ($T = 600\ °C$, $N_2 = 1\ L/min$, and the batch feeding was about 3.0 g) for liquid oil in a fixed-bed reactor. The detailed experimental methods can be referred to our previous study [30]. The physico-chemical property of the untreated biochar (U-char) was shown in Table 1. The micropore surface area, micropore volume, and nitrogen content were $224.12\ m^2/g$, 0.0734 ml/g, and 1.09 wt%, respectively. It indicated that this biochar did have not only the efficient micropore structure, but also the high nitrogen content.

### 2.2. Modification of the biochar

The biochar with the particle size of 0.6–1 mm was subjected to different modification methods with carbon dioxide, ammonia gas and their mixture. The modification process was illustrated as follows. Biochar particles (approximately 2.0 g) in a quartz reactor were treated in a vertical tube furnace. The biochar was heated up gradually to the preset temperature (500–900 °C, and the heating rate is 10 °C/min) with $N_2$ (99.99%; 400 ml/min) purging. After the temperature reached the desired value, $N_2$ was replaced by $CO_2$ (99.999%; 100 ml/min), ammonia (99.999%; 80 ml/min) or $CO_2$–ammonia ($CO_2 = 100\ ml/min$ and ammonia = 80 ml/min). During these treatments, biochars were kept at the final temperatures for 30 min. Finally, the furnace was cooled to the ambient temperature under the $N_2$ atmosphere. The modified biochars were labeled as C-char, A-char and CA-char accordingly.

### 2.3. Chemical and textural characterization

The nitrogen content of the raw and modified biochars was measured with CHNS elementary analyzer (Vario Micro cube, Germany). The organic species, especially N contained organic functional group of biochars were characterized using FTIR (VERTEX 70, Bruker, Germany) spectrometer at resolution of $4\ cm^{-1}$ equipped, and the apodization function was the Happ–Genzel type [30]. About 0.7 mg dried sample was mixed with 70 mg KBr to prepare the tablet by simultaneous pressing ($10\ tons/cm^2$ for 10 min). The physical properties of all biochars were analyzed with isothermal adsorption of carbon dioxide at 298 K (Micromeritics, ASAP 2020, USA). The $CO_2$ adsorption isotherm at relative pressures ($P/P_0$) ranging from $10^{-6}$ to 0.3 was used to calculate micropore structure. The micropore surface area ($S_{mic}$) and micropore volume ($V_{mic}$) were obtained by Dubinin–Radushkevich (DR) method.

### 2.4. $CO_2$ adsorption experiments

The $CO_2$ adsorption characteristics at 20 °C of the raw and modified biochar particles were calculated by the isothermal

**Table 1**
Physical and chemical properties of raw and modified biochars.

| Samples | $T$ (°C) | Surface area of micropore ($m^2/g$) | Micropore volume (ml/g) | Nitrogen content (wt.%) |
|---|---|---|---|---|
| U-char | 600 | 224 | 0.07 | 1.09 |
| C-char | 500 | 289 | 0.12 | 1.28 |
| | 600 | 351 | 0.13 | 1.02 |
| | 700 | 372 | 0.14 | 0.78 |
| | 800 | 610 | 0.24 | 0.54 |
| | 900 | 556 | 0.21 | 0.47 |
| A-char | 500 | 161 | 0.06 | 2.91 |
| | 600 | 252 | 0.10 | 3.48 |
| | 700 | 255 | 0.10 | 2.45 |
| | 800 | 349 | 0.14 | 1.61 |
| | 900 | 435 | 0.17 | 0.71 |
| CA-char | 500 | 95 | 0.04 | 3.78 |
| | 600 | 297 | 0.12 | 3.91 |
| | 700 | 336 | 0.13 | 2.89 |
| | 800 | 627 | 0.25 | 1.52 |
| | 900 | 469 | 0.19 | 0.96 |

adsorption of carbon dioxide (Micromeritics, ASAP 2020, USA). The $CO_2$ adsorption characteristics at 120 °C were investigated with a fixed bed adsorption system (Fig. 1). Approximately 5.0 g biochar particles was placed in the fixed bed reactor (Inner diameter = 15 mm), and heated up to 150 °C under pure $N_2$ flow (50 ml/min) and held isothermally for 2 h to remove the adsorbed water and other impurities. After that, the temperature was decreased to 120 °C, and then, $CO_2$ with the flow rate of 10 ml/min was introduced into the reactor, which was thereafter kept at 120 °C for the entire $CO_2$ adsorption experiment. The flow rates of $N_2$ and $CO_2$ were controlled with mass flow meters. A gas analyzer (HM-BX-T6, Huamin, China) was used to monitor the outlet concentration of $CO_2$.

### 2.5. Model description

To fit the breakthrough curve of adsorption, the deactivation model (DM) was introduced in the sight of adsorption dynamics. The first-order reaction on the sorbent surface was assumed to the adsorbent deactivation, and an index decline equation with time was supposed [31]. The deactivation model for the prediction of breakthrough curves in packed columns proposed was given as follows [32]:

$$\frac{C}{C_0} = \exp\left[\frac{1 - \exp[(k_0 W/Q)(1 - \exp(-k_d t))]}{1 - \exp(-k_d t)} \exp(-k_d t)\right] \qquad (1)$$

where, $C_0$ and $C$ are inlet and outlet concentrations of the tracer, respectively; $k_0$ is the initial sorption rate constant and $k_d$ is the deactivation rate constant; $W$ is weight of adsorbent and $Q$ is volumetric flow rate.

The $CO_2$ concentration was the average of three experimental data to reduce the relative errors, which were within ±5%. According to the adsorption breakthrough curves, the adsorption amount of the adsorbent is calculated.

## 3. Results and discussion

### 3.1. Chemical characterization

The FTIR spectra of the raw and $CO_2$ modified biochars were shown in Fig. 2a. It can be observed that the biochars presented some similar peaks at 3437 $cm^{-1}$, 2923 $cm^{-1}$ and 2856 $cm^{-1}$, which could be ascribed to phenol O—H, asymmetric and symmetric C—H stretching vibrations in aliphatic CH, $CH_2$, and $CH_3$, respectively [17,33]. In addition, the weak bands at 1450–1400 $cm^{-1}$ could be attributed to N—COO skeletal vibration [34], while the strong bands in the 1100–1000 $cm^{-1}$ region might be related to C—O stretching.

However, the ammonia modified biochars (shown in Fig. 2b) contain not only O—H (3421 $cm^{-1}$), C—O (1164 $cm^{-1}$), C—H (2923 and 2857 $cm^{-1}$), and N—COO (1416 $cm^{-1}$) functional groups, but also some other nitrogen-containing functional groups, such as C═N (1745–1586 $cm^{-1}$) and C—N (1056 and 1040 $cm^{-1}$) [17,24]. The broad band appearing at 3400 $cm^{-1}$ could be also due to the amine N—H stretching vibrations [34]. These additional adsorption peaks and bands confirmed that high temperature ammonia treatment did introduce some nitrogen functional groups to biochar surface. It might be attributed that ammonia was broken down into some radicals, such as $NH_2$, NH, and H at the high temperature, which reacted with surface oxides and active sites with N functional groups formed [16,17,35]. Nevertheless, the strong band in 1745–1586 $cm^{-1}$ region (attributed to oxime C═N—OH, pyridine C═N and C═O stretching) gradually reduced with the modified temperature increasing from 500 to 700 °C and disappeared at 800 °C. But, the aliphatic C—N stretching band at 1160–1040 $cm^{-1}$ emerges enormously at 800 °C, which is in accordance with previous studies [17]. It indicated that C═N and C═O groups would be converted to C—N groups with modified temperature increasing. That might be because the formation of some new C—N groups

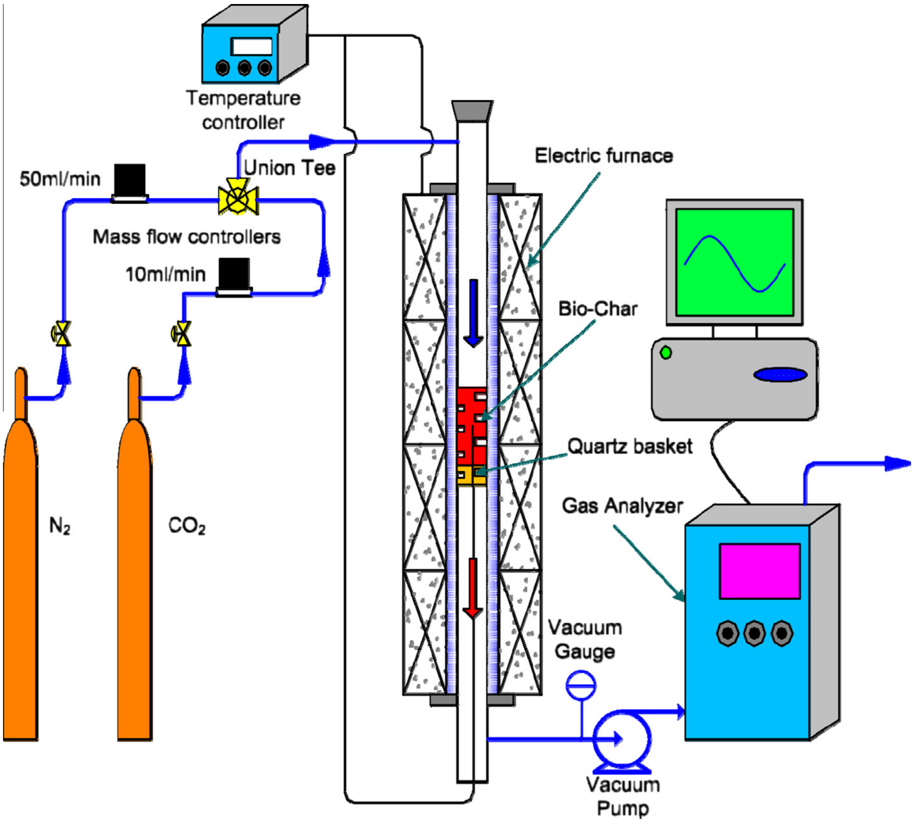

**Fig. 1.** The fixed bed adsorption system for $CO_2$ capture.

derived from reaction of $C{=}O$ groups with ammonia, or the transformation of $C{=}N$ bonds to a more stabilized single bond ($C{-}N$) at high temperatures.

In comparison with A-char, biochars treated with the combination of ammonia and $CO_2$ showed similar FTIR spectra (shown in Fig. 2c). Nevertheless, an obvious difference can be found on carbamate or carbamic acid ($N{-}COO$) skeletal vibration at 1410–1430 $cm^{-1}$, which increased with modification temperatures. The possible mechanisms were illustrated in Fig. 3. It indicated that the chemical reaction between amine and $CO_2$ might follow the reaction of $N{-}COO$ formation (shown in Fig. 3, Mechanism A [36,37]). Firstly, $C{-}OH$ and $C{-}O{-}C$ could respectively react with ammonia to generate the primary and secondary amines by Eqs. (a) and (b). Then, they could react with $CO_2$ and resulted in the formation of $N{-}COO$ through Eqs. (c) to (e). However, if the amine of $N{-}COO$ was secondary, dehydration reaction of the corresponding ammonium carbamate or the carbamic acid (shown in Fig. 3, Mechanism B [38–40]) can lead to the formation of pyridine $C{=}N$ and $C{=}O$ (lactones and ketones). Consequently, the production of pyridine $C{=}N$ and $C{=}O$ could probably provide more active sites for the introduction and conversion of nitrogen functional groups.

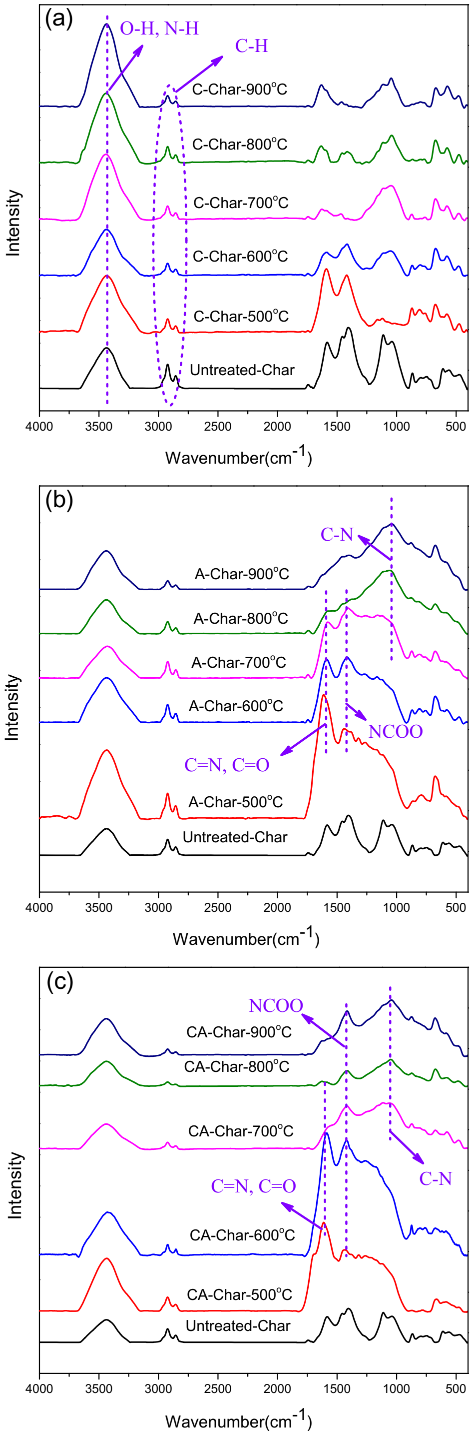

**Fig. 2.** FTIR spectra of C-chars (a), A-chars (b) and CA-chars (c) in comparisons with untreated char.

From the nitrogen content of the raw and modified biochars presented in Table 1, we can find that the nitrogen content of C-char gradually reduced with the increase of the modification temperature. However, compared with the C-char, the nitrogen contents of A-char and CA-char reached the maximum at 600 °C and then decreased with modification temperature increasing, and they were both higher than that of the C-char. It indicated that the nitrogen functional groups could be introduced onto the surface of biochar during the high temperature ammonia treatment, and these nitrogen functional groups began to decompose from 600 °C. In addition, the nitrogen content of CA-char was significantly higher than that of A-char at the same modification temperature. Combined with the FTIR spectra, it could be confirmed that the presence of $CO_2$ during the high temperature ammonia treatment could promote the ammonification and enrich the nitrogen-contained functional groups.

### 3.2. Textural characterization

The micropore structure of the biochar was also shown in Table 1. The surface area and volume of micropore for C-char and CA-char both increased with the modification temperature increasing from 500 °C to 800 °C. At 800 °C, their micropore surface areas reached the maximum (610.04 $m^2/g$ and 627.15 $m^2/g$, respectively); while with the temperature increasing to 900 °C, the

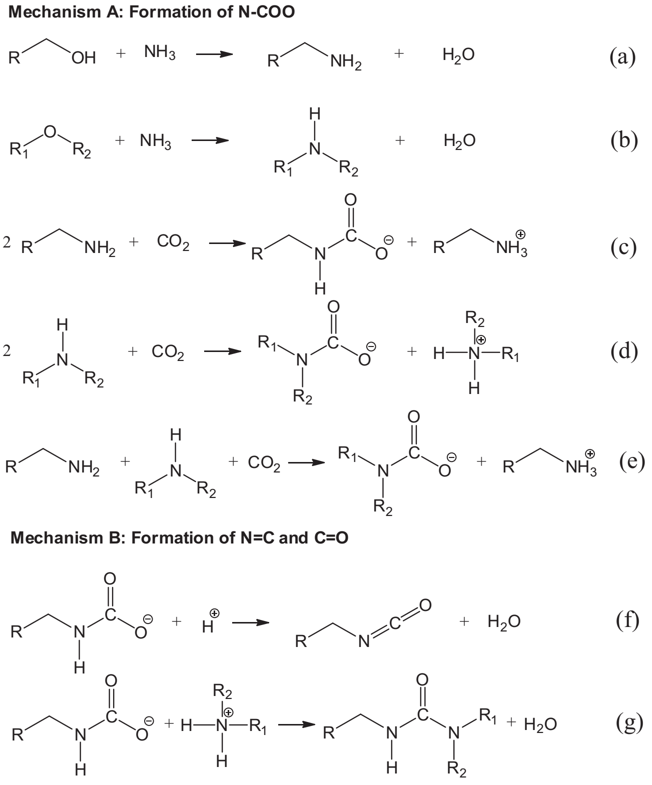

**Fig. 3.** Mechanisms for the reaction of ammonia and $CO_2$ with the biochar surface.

micropore surface area reduced greatly to 556.35 $m^2/g$ and 469.36 $m^2/g$, respectively. It might be attributed that the decomposition of some functional groups and carbon dioxide hot corrosion improved the pore structure significantly with $CO_2$ presence from 500 °C to 800 °C [41]. When the temperature was too high (>800 °C), some micropore might be overlapped, due to the inorganic melting and biochar gasification reaction with $CO_2$, which might result in the embrittlement and collapse of the carbon skeleton [42]. In addition, the micropore surface area of the CA-char-500 (when the modification temperature was 500 °C) was the least (94.52 $m^2/g$) among all modified biochars. The reason may be as follows. On the one hand, the modification temperature did not reach $CO_2$ activation temperature, and the effect of the micropore improvement was not obvious. On the other hand, $CO_2$ could combine with the biochar surface and generate a number of active sites that may prompt the introduction of the nitrogen containing functional groups (including urea and ammonium salt). When excessive nitrogen functional groups were introduced, it may block the micropore entrance and reduce the surface area. However, with the increase of modification temperature (>500 °C), $CO_2$ activation became more vigorous, and the micropore surface area and volume of CA-char would surpass A-char. It showed that although some micropore entrances could be blocked by nitrogen-containing functional groups (such as amino, pyrrole and pyridinic-like functional groups), the presence of $CO_2$ was benefit for improvement of the obstructed micropore when the modification temperature was beyond 500 °C.

### 3.3. $CO_2$ adsorption at 20 °C

The $CO_2$ adsorption properties of the raw and modified biochars at 20 °C were shown in Fig. 4a. When the modification temperature increased from 500 to 800 °C, the $CO_2$ adsorption capacity of the C-char increased significantly, and the maximum (99.42 mg/g) was obtained at 800 °C for C-char; after that (>800 °C), it decreased slightly with the modification temperature increasing further. It was possibly because that higher temperature was favorable for the formation of micropore structure of C-char (<800 °C), and the better micropore structure was more advantageous to the $CO_2$ adsorption at 20 °C. However, when the temperature was too high (>800 °C), some micropores may be coalesced to form mesopore or macropore [30]. Then the optimized micropore structure was destroyed, and it would weaken the adsorption capacity of $CO_2$ at 20 °C.

With respect to the $CO_2$ adsorption at 20 °C of CA-char and A-char, the similar varying tendency was displayed. However, their $CO_2$ adsorption capacity at 20 °C was different from each other. When the modification temperature increased from 700 to 900 °C, the $CO_2$ adsorption capacities at 20 °C of the C-char and CA-char were much higher than that of the A-char. It indicated that the better textural characterization, the larger $CO_2$ adsorption capacity. In addition, the $CO_2$ adsorption capacity of the CA-char-500 (500 °C) was the smallest among all biochars. It might be because that the modification temperature was too low, and $CO_2$ activation cannot take place.

### 3.4. $CO_2$ adsorption at 120 °C

The breakthrough curve of $CO_2$ adsorption on three different kinds of modified biochars at 120 °C was plotted in Fig. 5. It can be observed that the CA-char had the longest $CO_2$ breakthrough time (the time when the $CO_2$ concentration at the outlet reached 10% allowable breakthrough concentration), followed by A-char and C-char. It represented that the $CO_2$–ammonia modification was the most efficient treatment methods for $CO_2$ adsorption. When the modification temperature was between 500 and 900 °C, the breakthrough time of $CO_2$–ammonia adsorption followed the order of 600 > 500 > 700 > 800 > 900 °C. It illustrated that 600 °C was the optimal choice to produce CA-char for the $CO_2$ adsorption at 120 °C [43,44]. Compared with CA-char, A-char at the different modification temperatures had the similar breakthrough order, but C-char (the order of 800 > 900 > 500 > 600 > 700 °C) was very different with them. This difference mainly resulted from the generation and decomposition of nitrogen functional groups, and the change of micropore structure in the different modification temperatures.

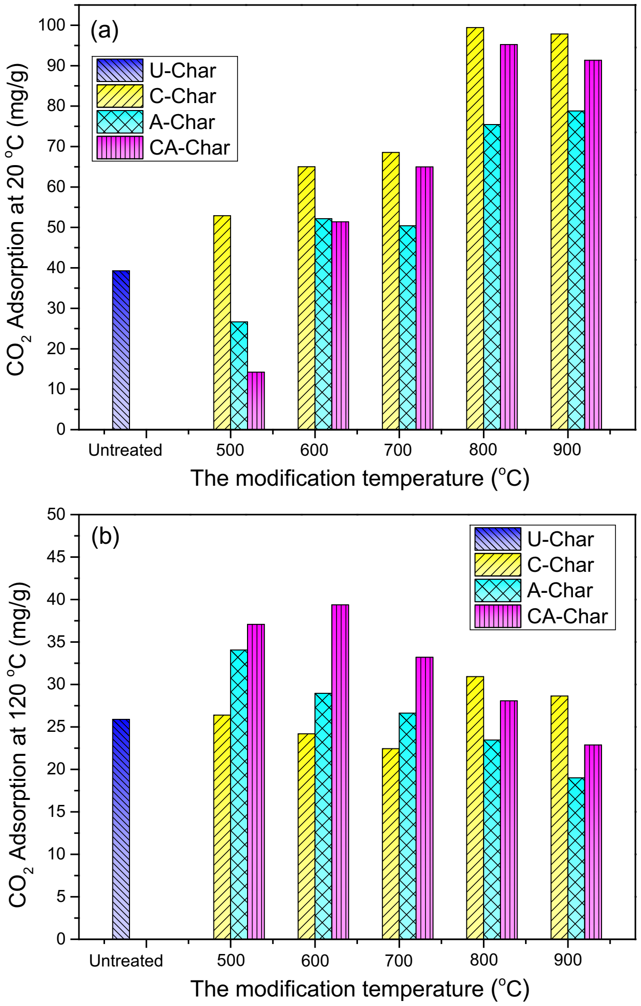

**Fig. 4.** The $CO_2$ adsorption capacity at 20 °C (a) and 120 °C (b) of different biochars.

The adsorption kinetics of $CO_2$ on raw and modified biochars with the initial adsorption rate constant ($k_o$) and deactivation rate constant ($k_d$) of the DM are showed in Table 2. With the increase of modification temperature, the initial adsorption rate constant of CA-char and A-char both increased firstly and then decreased, and their deactivation rate constant showed a tendency of increase. However, the change rules of $k_o$ and $k_d$ on C-char were exactly the opposite of CA-char and A-char. It probably suggested that high temperature ammonification was more advantageous to the $CO_2$ adsorption at 120 °C than the simple $CO_2$ activation. The correlation indexes ($R^2$) of all biochars were over 0.99, which showed that the proposed DM could well fit the $CO_2$ adsorption at 120 °C.

The breakthrough curve would be integrated versus time to obtain the $CO_2$ adsorption capacity at 120 °C (shown in Fig. 4b). The $CO_2$ adsorption capacity at 120 °C was very different from

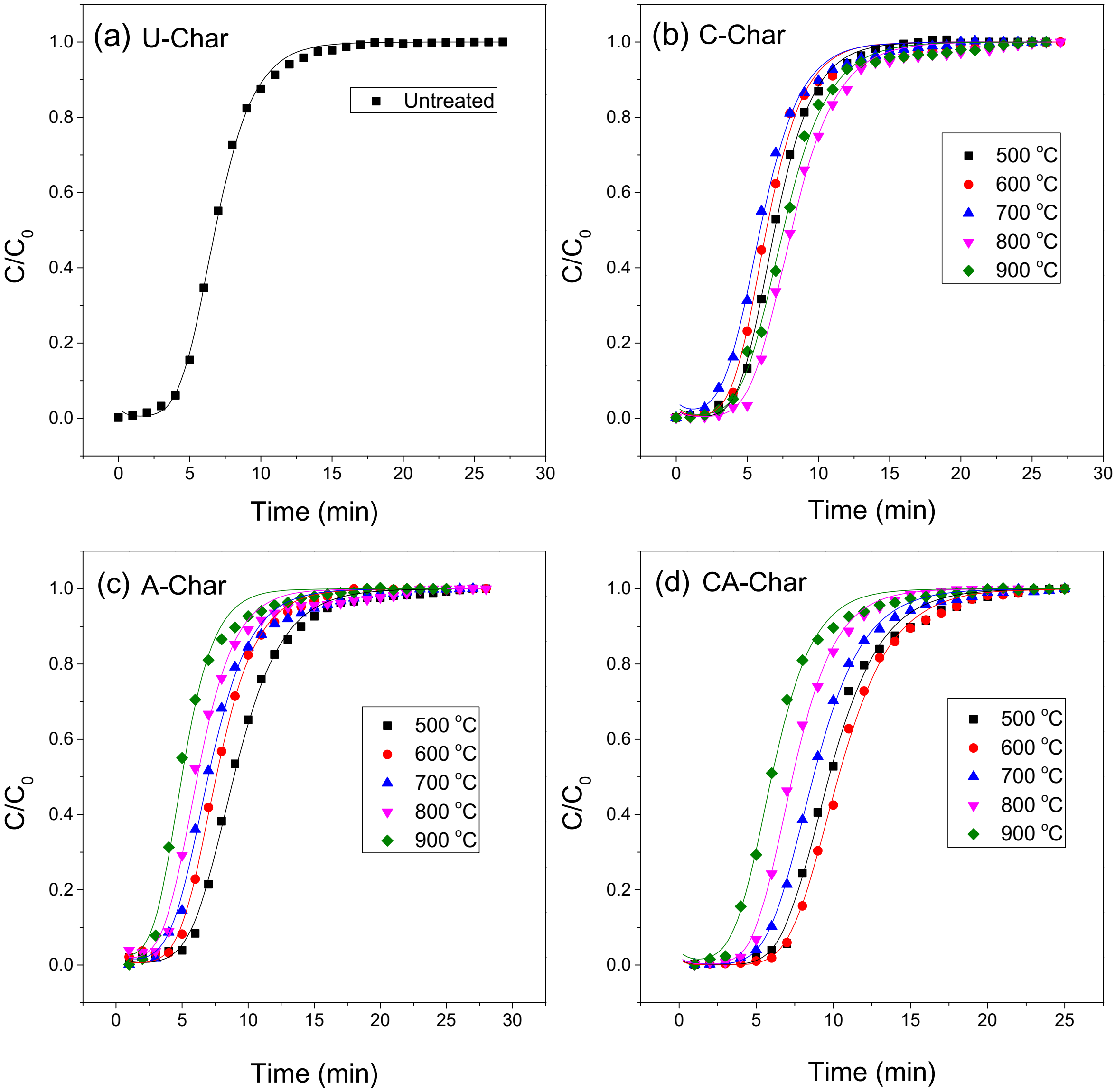

**Fig. 5.** Breakthrough behavior of $CO_2$ adsorption at 120 °C on the U-char (a), C-chars (b), A-chars (c) and CA-chars (d).

**Table 2**
The coefficients of deactivation model for the $CO_2$ adsorption at 120 °C.

| Samples | T (°C) | $R^2$ | $k_d$ ($min^{-1}$) | $k_o$ ($cm^3\ min^{-1}\ g^{-1}$) |
|---|---|---|---|---|
| U-char | 600 | 0.99903 | 0.571 | 43.112 |
| C-char | 500 | 0.99926 | 0.572 | 43.980 |
| | 600 | 0.99545 | 0.597 | 42.116 |
| | 700 | 0.99735 | 0.566 | 37.117 |
| | 800 | 0.99782 | 0.487 | 43.951 |
| | 900 | 0.99708 | 0.492 | 41.069 |
| A-char | 500 | 0.99818 | 0.431 | 42.755 |
| | 600 | 0.9989 | 0.510 | 43.038 |
| | 700 | 0.99542 | 0.505 | 39.210 |
| | 800 | 0.99361 | 0.559 | 38.252 |
| | 900 | 0.99252 | 0.661 | 36.705 |
| CA-char | 500 | 0.99665 | 0.453 | 49.158 |
| | 600 | 0.99886 | 0.439 | 50.626 |
| | 700 | 0.99909 | 0.475 | 46.078 |
| | 800 | 0.99874 | 0.558 | 45.678 |
| | 900 | 0.99705 | 0.588 | 39.267 |

those at 20 °C. The $CO_2$ adsorption capacity (120 °C) of the C-char firstly decreased gradually when the modification temperature increased from 500 to 700 °C, and then increased greatly at 800 °C. It was probably due to the gradual decomposition of nitrogen-containing functional groups and the improvement of micropore structure with the increase of the modification temperature. In comparison with the C-char, the $CO_2$ adsorption capacity at 120 °C on the CA-char firstly increased as the modification temperature below 600 °C, but when the modification temperature surpassed 600 °C, it gradually decreased. That was because that there were a large number of nitrogen functional groups to turn out when the modification temperature from 500 to 600 °C, but these nitrogen functional groups would begin to break down as the temperature exceeded 600 °C. In addition, although the CA-char and A-char were both treated in the high temperature ammonia, the $CO_2$ adsorption capacity on the CA-char was obviously larger than that on A-char, and the CA-char-600 presented the largest $CO_2$ adsorption capacity (39.37 mg/g). It showed a light that the CA-char could provide more active sites to adsorb $CO_2$.

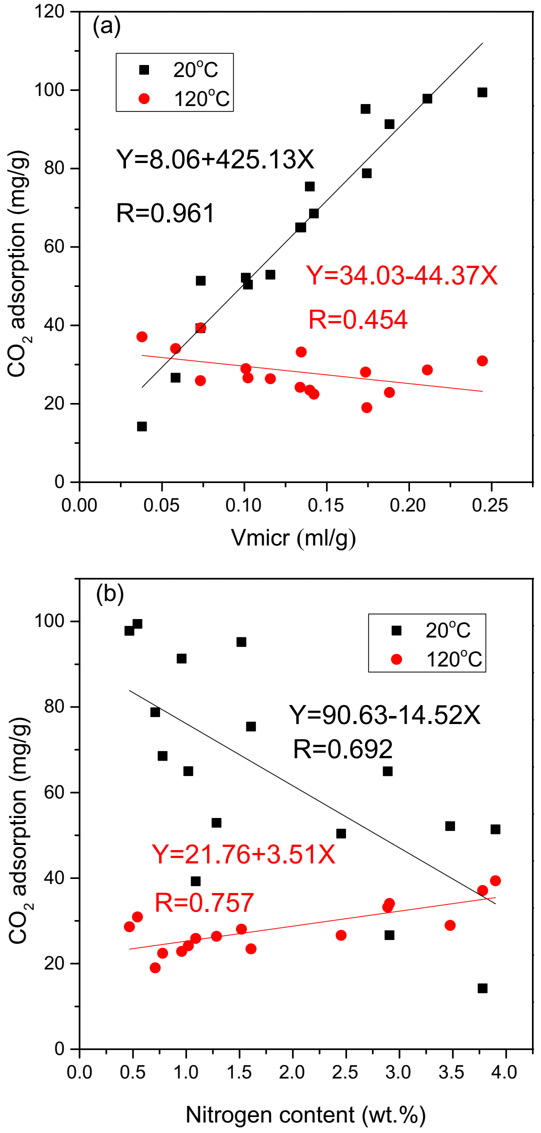

**Fig. 6.** Relationship between the adsorption capacity of different biochars and the micropore volume (a) and nitrogen content (b).

### *3.5. Effect of physical and chemical properties on $CO_2$ adsorption at different temperatures*

The effects of physical and chemical properties of the modified biochars on $CO_2$ adsorption at 20 and 120 °C were explored. The linear fitting of the scattered data was introduced to analyze the relationship of the micropore volume and nitrogen content with $CO_2$ adsorption. The results were shown in Fig. 6. It can be observed that when the adsorption temperature was 20 °C, the adsorption capacity increased with the increase of the micropore volume, but decreased with the enhancement of the nitrogen content. However, the opposite tendency was found when the adsorption temperature was up to 120 °C, *i.e.*, the $CO_2$ adsorption capacity slightly decreased with the micropore volume increasing, but increased with the nitrogen content increasing. At the lower adsorption temperature (20 °C), it demonstrated that the $CO_2$ adsorption capacity showed linear relationship with the micropore volume, but no obvious relation with the nitrogen content. It can be deduced that this process of the $CO_2$ adsorbed was mainly $CO_2$ filling in the microporous structure of the modified biochars, and Van der Wals forces were the dominant driving force for the $CO_2$ adsorption [45]. However, at the higher adsorption temperature (120 °C), no obvious relationship showed between $CO_2$ adsorption capacity and the micropore volume, whereas a much stronger relationship with the nitrogen content was prominent. It can be derived that this process was mainly the chemisorption by the nitrogen functional groups, and the surface chemistry characteristics might be the main factor to control the $CO_2$ adsorption at higher temperature.

## 4. Conclusions

The modification property of biochar derived from biomass fast pyrolysis with $CO_2$–ammonia modification was investigated, and the influence of physical and chemical properties on $CO_2$ adsorption behavior at different temperatures was explored as well. The main conclusions are as follows:

1. The high temperature activation treatment improved the micropore structure that could enhance the $CO_2$ adsorption at 20 °C. Meanwhile, in the high temperature process, the $CO_2$ presence is not only conducive to the micropore structure improvement, but also can introduce some hetero atom groups (such as C—O and C═O), and these hetero atom groups may provide more active sites for the introduction of nitrogen functional groups.
2. When the modification temperature from 500 to 600 °C, ammonia could react with the C-matrix of biochars, and introduce nitrogen functional groups, which was benefit to the $CO_2$ adsorption at 120 °C. However, when the modified temperature surpassed 600 °C, the nitrogen functional groups were gradually diminished, and it was adverse to the $CO_2$ adsorption at 120 °C.
3. The $CO_2$ adsorption capacity at 20 °C showed a linear correlation with micropore volume of biochar particles. However, it obviously depended on the nitrogen content in biochar at 120 °C, due to the chemical adsorption dominating the high temperature adsorption process.

## Acknowledgements

The authors wish to express their sincere thanks to the financial support from National Natural Science Foundation of China (51276075 and 51376076), and National Basic Research Program of China (2013CB228102).

## References

[1] P. Martin, C. Osvaldo, P. Jean, L. Paul, H. Clair, Climate Change 2007: Impacts, Adaptation and Vulnerability, first ed., Cambridge University Press, Cambridge, U.K., 2007.

[2] Z.E. Zhang, Y.F. Yan, L. Zhang, S.X. Ju, Hollow fiber membrane contactor absorption of $CO_2$ from the flue gas: review and perspective, Global Nest J. 16 (2014) 355–374.

[3] A.S. González, M.G. Plaza, F. Rubiera, C. Pevida, Sustainable biomass-based carbon adsorbents for post-combustion $CO_2$ capture, Chem. Eng. J. 230 (2013) 456–465.

[4] Z. Feng, F. Cheng-Gang, W. You-Ting, W. Yuan-Tao, L. Ai-Min, Z. Zhi-Bing, Absorption of $CO_2$ in the aqueous solutions of functionalized ionic liquids and MDEA, Chem. Eng. J. 160 (2010) 691–697.

[5] A. Ahmady, M.A. Hashim, M.K. Aroua, Density, viscosity, physical solubility and diffusivity of $CO_2$ in aqueous MDEA+ [bmim][$BF_4$] solutions from 303 to 333 K, Chem. Eng. J. 172 (2011) 763–770.

[6] A. Veawab, P. Tontiwachwuthikul, A. Chakma, Corrosion behavior of carbon steel in the $CO_2$ absorption process using aqueous amine solutions, Ind. Eng. Chem. Res. 38 (1999) 3917–3924.

[7] K. Jurewicz, K. Babeł, R. Pietrzak, S. Delpeux, H. Wachowska, Capacitance properties of multi-walled carbon nanotubes modified by activation and ammoxidation, Carbon 44 (2006) 2368–2375.

[8] A. Bhatnagar, W. Hogland, M. Marques, M. Sillanpää, An overview of the modification methods of activated carbon for its water treatment applications, Chem. Eng. J. 219 (2013) 499–511.

[9] P. Nowicki, R. Pietrzak, Effect of ammoxidation of activated carbons obtained from sub-bituminous coal on their $NO_2$ sorption capacity under dry conditions, Chem. Eng. J. 166 (2011) 1039–1043.

[10] Z. Zhang, M. Xu, H. Wang, Z. Li, Enhancement of $CO_2$ adsorption on high surface area activated carbon modified by $N_2$, $H_2$ and ammonia, Chem. Eng. J. 160 (2010) 571–577.

[11] F. Adib, A. Bagreev, T.J. Bandosz, Adsorption/oxidation of hydrogen sulfide on nitrogen-containing activated carbons, Langmuir 16 (2000) 1980–1986.

[12] A. Meyer-Plath, K. Schröder, B. Finke, A. Ohl, Current trends in biomaterial surface functionalization-nitrogen containing plasma assisted processes with enhanced selectivity, Vacuum 71 (2003) 391–406.

[13] A. Heydari-Gorji, A. Sayari, $CO_2$ capture on polyethylenimine-impregnated hydrophobic mesoporous silica: experimental and kinetic modeling, Chem. Eng. J. 173 (2011) 72–79.

[14] S.H. Khalil, M.K. Aroua, W.M.A.W. Daud, Study on the improvement of the capacity of amine-impregnated commercial activated carbon beds for $CO_2$ adsorbing, Chem. Eng. J. 183 (2012) 15–20.

[15] C.S. Lee, Y.L. Ong, M.K. Aroua, W.M.A.W. Daud, Impregnation of palm shell-based activated carbon with sterically hindered amines for $CO_2$ adsorption, Chem. Eng. J. 219 (2013) 558–564.

[16] J. Przepiórski, M. Skrodzewicz, A.W. Morawski, High temperature ammonia treatment of activated carbon for enhancement of $CO_2$ adsorption, Appl. Surf. Sci. 225 (2004) 235–242.

[17] M.S. Shafeeyan, W.M.A.W. Daud, A. Houshmand, A. Arami-Niya, Ammonia modification of activated carbon to enhance carbon dioxide adsorption: effect of pre-oxidation, Appl. Surf. Sci. 257 (2011) 3936–3942.

[18] A. Vesel, I. Junkar, U. Cvelbar, J. Kovac, M. Mozetic, Surface modification of polyester by oxygen- and nitrogen-plasma treatment, Surf. Interface Anal. 40 (2008) 1444–1453.

[19] F. Bretagnol, M. Tatoulian, F. Arefi-Khonsari, G. Lorang, J. Amouroux, Surface modification of polyethylene powder by nitrogen and ammonia low pressure plasma in a fluidized bed reactor, React. Funct. Polym. 61 (2004) 221–232.

[20] S. Zheng, W. Jiang, Y. Cai, D.D. Dionysiou, K.E. O'Shea, Adsorption and photocatalytic degradation of aromatic organoarsenic compounds in $TiO_2$ suspension, Catal. Today 224 (2014) 83–88.

[21] F. Rodriguez-Reinoso, M. Molina-Sabio, Activated carbons from lignocellulosic materials by chemical and/or physical activation: an overview, Carbon 30 (1992) 1111–1118.

[22] S.J. Allen, E. Ivanova, B. Koumanova, Adsorption of sulfur dioxide on chemically modified natural clinoptilolite. Acid modification, Chem. Eng. J. 152 (2009) 389–395.

[23] J.P. Boudou, M. Chehimi, E. Broniek, T. Siemieniewska, J. Bimer, Adsorption of $H_2S$ or $SO_2$ on an activated carbon cloth modified by ammonia treatment, Carbon 41 (2003) 1999–2007.

[24] S.M. Mahurin, J.S. Lee, X. Wang, S. Dai, Ammonia-activated mesoporous carbon membranes for gas separations, J. Membr. Sci. 368 (2011) 41–47.

[25] C.L. Mangun, K.R. Benak, J. Economy, K.L. Foster, Surface chemistry, pore sizes and adsorption properties of activated carbon fibers and precursors treated with ammonia, Carbon 39 (2001) 1809–1820.

[26] N.O. Nelson, S.C. Agudelo, W. Yuan, J. Gan, Nitrogen and phosphorus availability in biochar-amended soils, Soil Sci. 176 (2011) 218–226.

[27] K.Y. Chan, L. Van Zwieten, I. Meszaros, A. Downie, S. Joseph, Agronomic values of greenwaste biochar as a soil amendment, Aust. J. Soil Res. 45 (2007) 629–634.

[28] H. Tuo, Thermal-economic analysis of a transcritical Rankine power cycle with reheat enhancement for a low-grade heat source, Int. J. Energy Res. 37 (2013) 857–867.

[29] A.E. Creamer, B. Gao, M. Zhang, Carbon dioxide capture using biochar produced from sugarcane bagasse and hickory wood, Chem. Eng. J. 249 (2014) 174–179.

[30] Y. Chen, H. Yang, X. Wang, S. Zhang, H. Chen, Biomass-based pyrolytic polygeneration system on cotton stalk pyrolysis: influence of temperature, Bioresour. Technol. 107 (2012) 411–418.

[31] T. Kopaç, S. Kocabaş, Adsorption equilibrium and breakthrough analysis for sulfur dioxide adsorption on silica gel, Chem. Eng. Process. 41 (2002) 223–230.

[32] S.W. Park, B.S. Choi, J.W. Lee, Breakthrough data analysis of adsorption of toluene vapor in a fixed-bed of granular activated carbon, Sep. Sci. Technol. 42 (2007) 2221–2233.

[33] W. Jiang, M. Pelaez, D.D. Dionysiou, M.H. Entezari, D. Tsoutsou, K. O'Shea, Chromium(VI) removal by maghemite nanoparticles, Chem. Eng. J. 222 (2013) 527–533.

[34] M.S. Shafeeyan, W.M.A.W. Daud, A. Houshmand, A. Shamiri, A review on surface modification of activated carbon for carbon dioxide adsorption, J. Anal. Appl. Pyrolysis 89 (2010) 143–151.

[35] M.G. Plaza, C. Pevida, A. Arenillas, F. Rubiera, J.J. Pis, $CO_2$ capture by adsorption with nitrogen enriched carbons, Fuel 86 (2007) 2204–2212.

[36] Y.G. Ko, S.S. Shin, U.S. Choi, Primary, secondary, and tertiary amines for $CO_2$ capture: designing for mesoporous $CO_2$ adsorbents, J. Colloid Interface Sci. 361 (2011) 594–602.

[37] V. Zeleňák, M. Badaničová, D. Halamová, J. Čejka, A. Zukal, N. Murafa, G. Goerigk, Amine-modified ordered mesoporous silica: effect of pore size on carbon dioxide capture, Chem. Eng. J. 144 (2008) 336–342.

[38] A. Sayari, A. Heydari-Gorji, Y. Yang, $CO_2$-induced degradation of amine-containing adsorbents: reaction products and pathways, J. Am. Chem. Soc. 134 (2012) 13834–13842.

[39] P.N. Sutar, A. Jha, P.D. Vaidya, E.Y. Kenig, Secondary amines for $CO_2$ capture: a kinetic investigation using N-ethylmonoethanolamine, Chem. Eng. J. 207–208 (2012) 718–724.

[40] H. Yang, Y. Yuan, S.C.E. Tsang, Nitrogen-enriched carbonaceous materials with hierarchical micro-mesopore structures for efficient $CO_2$ capture, Chem. Eng. J. 185–186 (2012) 374–379.

[41] M. Molina-Sabio, M. Gonzalez, F. Rodriguez-Reinoso, A. Sepulveda-Escribano, Effect of steam and carbon dioxide activation in the micropore size distribution of activated carbon, Carbon 34 (1996) 505–509.

[42] M.M. Mahamud, Textural changes during $CO_2$ activation of chars: a fractal approach, Appl. Surf. Sci. 253 (2007) 6019–6031.

[43] M. Auta, N.D. Amat Darbis, A.T. Mohd Din, B.H. Hameed, Fixed-bed column adsorption of carbon dioxide by sodium hydroxide modified activated alumina, Chem. Eng. J. 233 (2013) 80–87.

[44] S. García, M.V. Gil, C.F. Martín, J.J. Pis, F. Rubiera, C. Pevida, Breakthrough adsorption study of a commercial activated carbon for pre-combustion $CO_2$ capture, Chem. Eng. J. 171 (2011) 549–556.

[45] A. Arenillas, K.M. Smith, T.C. Drage, C.E. Snape, $CO_2$ capture using some fly ash-derived carbon materials, Fuel 84 (2005) 2204–2210.